Zhou, Y, Li, L, Chen, Z, Rao, L, Ren, X, Xing, X and Yang, Q

Accidental damaged diamond-like carbon coating by prefabricated scratches: Experimental exploration on anticorrosion and tribological performances

Accidental damaged diamond-like carbon coating by prefabricated scratches: Experimental exploration on anticorrosion and tribological performances

Yefei Zhou [a,b,c], Lulu Li [a,c], Zhihao Chen [a,c], Lixiang Rao [b,c], Xuejun Ren [d], Xiaolei Xing [a,b,c],*, Qingxiang Yang [b,c],*

[a] *School of Mechanical Engineering, Yanshan University, Qinhuangdao 066004, PR China*
[b] *State Key Laboratory of Metastable Materials Science & Technology, Yanshan University, Qinhuangdao 066004, PR China*
[c] *Key Laboratory of Self-Lubricating Spherical Plain Bearing technology of Hebei Province, Yanshan University, Qinhuangdao 066004, PR China*
[d] *School of Engineering, Liverpool John Moores University, Liverpool L3 3AF, UK*

Abstract: Accidental damage on the diamond-like carbon (DLC) coating can have a great influence on the anticorrosion and tribological performances. In this study, DLC coating was deposited by a DC unbalanced magnetron sputtering technique. The scratch tests with different damage loads of 2, 10, 20, 30, 40 and 50 N were used to imitate the different types of accidental damage. The influence of different types of surface damage states on anticorrosion performance and scratch damage structures on tribological performance were studied and compared with those of the coating without damage. Cracking or spalling of the coating promotes the corrosion failure of the coating system and pitting corrosion of the stainless steel substrate, resulting in the deterioration of the corrosion protection effectiveness. With the damage increases from fine crack to complete failure, the corrosion resistance decrease obviously and the corrosion rate increases from 1.796×10^{-9} to 2.880×10^{-8} (A/cm^2). The coating with an appropriate scratch structure as the sample S2 (scratch width of 0.012 mm and the ratio of the scratch width to the contact width is 0.033) can effectively avoid the softening of the coating surface caused by graphitization and collect the wear debris particles, resulting in the excellent tribological behaviors with the lowest wear rate of 1.848×10^{-16} $m^3/(N \cdot m)$.

1. Introduction

Diamond-like carbon (DLC) coating, consisted of the C–C sp2 structure of graphite and the C–C sp3 structure of diamond, has attracted much attention from many scholars and is widely used in engineering parts due to the excellent performance of high corrosion resistance, high hardness and low friction coefficient [1–3]. Many scholars have pointed out that DLC coating can effectively improve the corrosion resistance and tribological behavior of 304 stainless steel [4–6]. The DLC coating makes stainless steel exhibiting an even better excellent performance in engineering applications. On the basis of a single DLC coating, the transition layer and multilayer structure are designed to improve the adhesion strength and further promote the tribological behavior [7–14]. Li et al. [7] investigated the addition of Cr interlayer and design of multilayer structure to improve the adhesion strength, tribological and corrosion performance of carbon film coated substrate. Shahsavari et al. [10] demonstrated that the DLC films with 40 nm Cr interlayer generated the higher adhesion strength, tribological performance and the highest hardness. Ma et al. [11] showed that multi-layers is one of the best ways to improve mechanical properties, wear and corrosion resistance compared with single layer coatings. Wang et al. [14] showed that the adhesion strength of the GLC film could be improved effectively by Cr interlayer design under sliding-friction. Due to the hardness, elasticity modulus and thermal expansion coefficient close to the metal substrate, and the property of easily forming metal carbide, the Cr transition layer plays an important role in improving the adhesion strength and the corrosion protection of the DLC coating on stainless steel in an aggressive marine environment. However, DLC coated stainless steel parts may be associated with abnormal surface conditions such as coating scratches, cracking or spalling and these are produced during transportation or the assembly process. The influence of accidental damage, due to the abnormal service, on the corrosion resistance and tribological behavior of DLC coating has been little studied by researchers. After accidental damage, the DLC coating surface will change from a continuous and complete state to a discontinuous and incomplete state. Researchers replicated the discontinuous and incomplete surface and further investigated the tribological behavior of the DLC coating [15–17]. He et al. [15] fabricated the textured DLC coatings by masking the substrate with metallic meshes and compared the tribological behaviors of the textured DLC coatings with the un-textured ones. The results showed that the textured DLC coating with a micro-dimples density of 52% exhibited the lowest average coefficient of friction (COF) and wear rate, both under dry friction and liquid lubrication conditions. Some researchers created the texture on the substrate by using a laser and then deposited the DLC coating on the polished substrate surface. Arslan et al. [16] evaluated the tribological performance of textured amorphous hydrogenated DLC coated surfaces, with various texture diameters and depths, under oil lubricated sliding conditions. The results indicated that the performance was significantly enhanced in the case of dimple diameter and depth of 100 μm and 6 μm, respectively. Shum et al. [17] compared the tribological properties of different textured DLC coatings and showed that DLC coating with the appropriate dimple density (10%) and diameter (100 mm) demonstrated a lower coefficient of friction and wear rate than that of the un-textured DLC coating. However, considering the discontinuity of the coating surface, the surface morphology of the coating under the above preparation process is different from that after accidental damage, so the research results of a textured DLC coating cannot fully support the service performance of the DLC coating after accidental damage. Therefore, another process needs to be applied to simulate the discontinuous coating surface after accidental damage. The coating cracking and peeling caused by accidental damage are

similar to those caused by the scratch test. In this paper, DLC nanocomposite coatings are fabricated on AISI 304 stainless steel by the ion beam assisted enhanced unbalanced magnetron sputtering technology. The scratch parameters, with different damage characteristics, are firstly determined by a progressive stress scratch test. On this basis, the role of different types of damages on the corrosion protection ability and tribological behavior of the DLC coatings are systematically investigated. Meanwhile, the relevant mechanism is also discussed in terms of the coating structure.

2. Experimental

2.1. Coating fabrication

The multilayer DLC coating was deposited on the polished 304 stainless steel sheets (15 mm × 15 mm × 3 mm) by the ion beam assisted enhanced unbalanced magnetron sputtering technology. The stainless steel substrates were ultrasonically cleaned with acetone and dried with dry nitrogen. The base pressure and temperature of the chamber were 6.0×10^{-1} Pa and around 100 ◦C, respectively. Before the deposition, all the substrates were pre-cleaned with Ar+ ions (plasma flow 20 sccm) for 30 min at a bias voltage of -600 V to get rid of the large particulate impurities and oxidizing contaminants. During the deposition process, the high purity Cr target (99.99%) and graphite target (99.99%), with the size of 85 mm × 245 mm × 10 mm, were used to fabricate the DLC nanocomposite (Cr/CrC/DLC) coating. The Cr and CrC transition layers were deposited to improve the adhesion of the DLC coating. The specific deposition process parameters are shown in Table 1.

2.2. Surface scratch prefabrication

The surface scratch of the DLC coating was prefabricated by a large load scratch tester (CSM Instruments Revetest) with a diamond cone head (radius = 200 μm, cone angle = 120◦). A linearly increasing normal loading force from 0 N to 60 N was employed in advance to characterize the loading force bearing capacity of the coating. Fig. 1 shows the scratch tracks of the DLC coating. The values of Lc1 (critical load of fine crack occurrence) was 5.5 ± 0.3 N and Lc2 (critical load when the coating begins to peel off) can be seen at the load of 18.3 ± 0.9 N. The excellent adhesion behavior of the coating with 48.3 ± 2.5 N (Lc3 complete failure) can be also observed. Scratch tests, with different constant scratch loads, are used to characterize different types of accidental damages. To investigated the influence of different accidental damages (from fine crack occurrence to complete failure) on the coating properties, six groups of the constant scratch loads (2, 10, 20, 30, 40 and 50 N) were chosen by referring to the scratch results in Fig. 1. In each group, three parallel scratches with the length of 3 mm were produced and the interval between adjacent two parallel scratches was 1 mm. Fig. 2 shows the surface state of the DLC coating for the corrosion resistance and tribological performance tests. The coatings with the constant scratch loads of 2, 10, 20, 30, 40 and 50 N are labelled as S1, S2, S3, S4, S5 and S6, respectively. The scratch free coating, labelled as S0, was used to compare with those of the other DLC coatings.

2.3. Corrosion test

The corrosion test was carried out by electrochemical measurements with the CHI660E electrochemical workstation and a conventional three-electrode system, which contained a saturated calomel electrode as the reference electrode (RE), a platinum sheet as the counter electrode (CE) and the tested coatings as the working electrode (WE). The test area was 13

mm2 covering three scratches. The 3.5 wt% NaCl solution was selected as the electrolyte, and the anticorrosion properties of the DLC coatings were analyzed by potentiodynamic polarization and electrochemical impedance spectroscopy (EIS) technology. The polarization potential was acquired from - 1.0 V to 1.0 V at a scan rate of 0.001 V/s. For comparison, the test was also performed on the 304 stainless steel substrate. The EIS test was performed with the frequency from 10^5 Hz to10^{-2} Hz and the amplitude of 10 mV. The EIS data were analyzed with the ZSimDem3.30 software and modelled by a proper electrical equivalent circuit. The surface morphologies after the potentiodynamic polarization tests were observed by scanning electron microscope (SEM, Phenom).

2.4. Tribological test

A reciprocating test with a transverse sliding direction, passing three scratches, was used to evaluate the friction and wear performance of the DLC coatings with prefabricated scratches. The corresponding applied load, frequency, sliding amplitude, test cycles and grinding pair were 5 N, 2.5 Hz, 3 mm, 10,000 cycles and GCr15 steel ball (diameter = φ3 mm), respectively. Before the tribological test, the coatings and GCr15 grinding pair were cleaned with acetone to remove the surface contaminants. At the beginning of the test, the contact pressure was 0.112 GPa, which was calculated by the following equation:

$$\frac{1}{E} = \left(\frac{1 - V_1^2}{E_1} + \frac{1 - V_2^2}{E_2}\right) \quad (1)$$

$$a = \left(\frac{3R}{4E}\right)^{\frac{1}{3}} W^{\frac{1}{3}} \quad (2)$$

$$\sigma = \frac{W}{\pi a^2} \quad (3)$$

where E, E_1, and E_2 are the comprehensive elastic modulus, and elastic modulus of the grinding pair and coating (GPa); V_1 and V_2 are the Poisson's ratios of the grinding pair and coating; a and R are the contact radius and grinding pair radius (μm); W is the applied load (N); and σ is the Hertzian contact stress (GPa).

After the sliding process, the surface morphologies were measured by confocal microscopy (Anton Paar, Conscan) and the wear rate was calculated by the following equation:

$$K = \frac{V}{FS} \quad (4)$$

where V, F, and S are the loss wear volume (m^3), applied load (N), and the sliding distance (m), respectively. The above corrosion and tribological tests were both repeated four times.

The microstructure of the wear tracks (non-scratching region on wear tracks) was analyzed by visible Raman spectrum with a 532 nm laser and a detection range from 500 to 2500 cm^{-1}. The microscopic morphologies were also observed by scanning electron microscope (SEM, Phenom). For the mechanical properties, the hardness and the elasticity modulus of the wear tracks (non-scratching region on wear tracks) on the coatings after the tribological test were accurately calculated by the nano-indentation tester (Anton Paar, NHT2) using a Berkovich indenter with 1 mN load. The measured results were averaged over 4 different regions of each

coating and these were detected with the depth controlled within 100 nm to avoid the effect of the stainless steel substrate.

3. Results and discussion

3.1. Anticorrosion properties

Potentiodynamic polarization curve can be used to evaluate the corrosion resistance of the DLC coatings and the measured results are presented in Fig. 3. It can be divided into two parts: cathode polarization and anode polarization. The intersection point of cathode polarization and anode polarization is the equilibrium state of the whole system and this can be analyzed through two factors: corrosion potential (E_{corr}) and corrosion current (I_{corr}). Meanwhile, the polarization resistance (Pol R) is associated with the dynamic characteristics of the whole electrode process at the electrode potential of E_{corr}. Table 2 shows the specific polarization parameters of all the samples. The Pol R of the coated samples is significantly higher than that of the bare substrate, indicating that the coating can act as a barrier to effectively protect the stainless steel substrate in a corrosive environment. The E_{corr} and I_{corr} of the sample S0 are - 0.190 V and 1.181×10^{-9} (A/cm^2), respectively. Compared with that, all the damaged samples reveal a lower Ecorr. With the accidental damage on the coating surface increasing to the degree of completely peels off, the stainless steel substrate in the damaged area is completely exposed to the corrosive environment, resulting in an obviously decrease in the E_{corr}. However, due to the scratch depth of the sample S1 is smaller than the thickness of the coating, the lowest E_{corr} value of the sample S1(-0.261 V) may be attributed to that fine cracks on the sample surface propagate to the CrC transition layer. It has been proven that the lower I_{corr} represent the better corrosion resistance with a slower reaction process [18,19]. For the samples S1–S6, the corrosion current increase from 1.796×10^{-9} to 2.880×10^{-8} (A/cm^2), which indicates higher corrosion rate with the increasing accidental damage on the coating surface. In addition, the evolution of the breakdown potential (potential at which it breaks, and the current remains unchanged with potential) is also consistent with the anticorrosion properties of the samples S1–S6.

To further analyse the anticorrosion properties of the samples S0–S6, EIS was used to effectively detect the coating structures exposed to the corrosive environment. Fig. 4 displays the evolution of the Bode-phase, Bode-impedance and Nyquist curves, varying with frequency. From Fig. 4(a), it can be seen that the angles varying with frequency show different tendencies for the samples S0–S6. In the curves, the phase angles close to -90°, 0° and 90° are regarded as the elements similar to capacitance, resistance, and inductance, respectively. Two time constants are observed in the curves of the samples S0–S6. The constants of the sample S0 at high frequency (105 Hz) and low frequency (1 Hz) are associated with the charge transfer processes at the coating/electrolyte interface and the stainless steel/electrolyte interface. It has a certain guiding significance for the equivalent circuit fitting of the coatings. For the sample S1, the curve basically displays the same impedance performance for the sample S0. It is worth noting that the phase angle curves of the samples S2–S6 change greatly with the frequency. Compared with the samples S0 and S1, the capacitance impedance of samples S2–S6 is more lower at high frequency regime and the high frequency (105 Hz) is associated with the solution resistance. The frequency associated with the charge transfer process at the coating/electrolyte interface gradually decreases with the increasing accidental damage on the coating surface. The frequency of the samples S2–S6 is around 3500, 1500, 1000, 600 and 300 Hz, respectively. Meanwhile, the resistance response in the middle frequency shows a significant decrease, which

might be attributed to the coating cracking or peeling. For the charge transfer process associated with the stainless steel/electrolyte interface, not obvious frequency difference is observed for all the samples.

For the Bode-impedance curves in Fig. 4(b), the slopes close to -1, 0, and 1 are regarded as the elements similar to capacitance, resistance, and inductance, respectively. For all the samples, the capacitance and the resistance are connected in parallel, and the total impedance can be expressed as:

$$|Z| = \frac{R}{\sqrt{1 + (\omega RC)^2}} \quad (5)$$

where R and C represents the resistance and capacitance, and ω is the frequency.

At 10^{-2} Hz, the total impedance value indicates the corrosion resistance of the samples [20,21]. The sample S0 exhibits the highest Log|Z|, indicating an excellent anticorrosion property. For other samples, the impedance value shows a significant decline with the increasing accidental damage on the coating surface, resulting in a decreasing corrosion protection ability. Comparing the Bode curves, the solution resistance can be detected at 105 Hz for the samples S2–S6 and this is different from the samples S0–S1. Fig. 4(c) shows the real part (Zreal) and the imaginary part (Zimag) of the impedance (|Z|) varying with frequency. At the same frequency, the poor capacitive resistance with a lower capacitive arc can be observed for the samples S1–S6, indicating a weakened anticorrosion ability compared with the S0 sample.

To fit the physical response detected from the impedance spectra, the reasonable circuit model is also shown in Fig. 4(d). The equivalent circuit consists of the solution resistance (Rs) in series with two hierarchical parallel RC circuits, where CPE_1 and R_1 represent the capacitance behavior of the coating/electrolyte interface and the resistance of the coating, CPE_2 and R_2 represent the double layer capacitance of the stainless steel/electrolyte interface and the charge transfer resistance, respectively. Due to the roughness of the coating surface, the constant phase element CPE is used to represent the capacitance and this can be expressed as:

$$Z_{CPE} = \frac{1}{Y_o(j\omega)^n} \quad (6)$$

where *Yo* represents the admittance of CPE, the data of *Yo*, just like C, is used to describe the data of C ($\Omega^{-1}cm^{-2}s^{-n}$), and n is the dimensionless index of how far the CPE elements deviate from ideal capacitance [22,23].

The specific parameters obtained from the circuits are shown in Fig. 5. The solution resistance (Rs) value is about 265.5 Ω. It has been reported that the R_1 value represents the resistance of the coating to prevent the electrolyte from penetrating through the defects [24]. A higher R_1 and lower CPE_1 value jointly improve the anticorrosion property of the coating system. It is clear that the accidental damage on the coating surface significantly reduce the corrosion resistance of the coating system. As shown in Fig. 5(a) and (b), the sample S0 without accidental damage presents the highest R1 value of 2.668×10^4 Ω cm2 and lowest CPE1 value of 3.434×10^{-9} F/cm2. Compared with that, the R_1 values of the samples S1–S6 sharply decrease from 2.084×10^4 Ω cm^2 to 1.400×10^3 Ω cm^2 and the CPE^1 values increase from 3.642×10^{-9} F/ cm^2 to 8.270

$\times 10^{-6}$ F/cm^2, indicating the degraded corrosion resistance. Meanwhile, in Fig. 5(c) and (d), the R2 value decrease from 5.447×10^8 Ω cm^2 to 1.840×10^7 Ω cm^2 and the CPE_2 increase from 1.495×10^{-7} F/cm^2 to 1.026×10^{-6} F/cm^2. The value evolutions are consistent with those of R_1 and CPE_1. The R_2 and the CPE_2 values also display the vulnerability of the stainless steel substrate to be corroded and the deteriorating corrosion protection effectiveness of the coating system. In 3.5 wt% NaCl solution, the coating cracking or peeling caused by the accidental damage allows the corrosive media to more easily penetrate the coating, resulting in the degraded corrosion resistance. Meanwhile, the stainless steel substrate surface exposed to the solution accelerates the corrosion process.

To display the influence of coating cracking or peeling on the corrosion resistance, Fig. 6 shows the SEM morphologies of the coatings after the potentiodynamic polarization test, and the image of the corroded bare stainless steel substrate is also provided for comparison. For the sample S0, no changes can be observed on the coating surface. Meanwhile, the more irregular convex areas can be obviously detected in the damaged areas of the samples S1–S6 and these are consistent with that of the bare stainless steel substrate. In order to further analyse the phenomena, an irregular convex area on the sample S2 is selected for EDS element analysis, where strong signals of Fe, Cr, O are detected. Comparing the interference of Cr in the coating, more Cr accumulate in the detected area. The accumulation of the above elements and the location of the detected area (strong C signal before potentiodynamic polarization test) jointly demonstrate the corrosion oxidation reaction of the exposed stainless steel substrate.

The related corrosion mechanism is shown in Fig. 6(i). The appearance of this kind of corrosion originates from pitting corrosion of the stainless steel, which involves two important processes: nucleation and development. Pitting is caused by the competitive adsorption of chlorine and oxygen in oxide film [25]. When chloride ions are selectively adsorbed around the cation lattice of the oxide film and replace the water molecules, the soluble chloride can be formed by the reaction of the chloride ions and the cations in the oxide film. The process promotes the metal ions to dissolve into the solution and makes the newly exposed metal form a small etch pit (pitting nuclei) at a specific point. Then the development process is closely related to the corrosion reaction of Fe and Cr and this can be express as:

$$\begin{aligned} Fe &\rightarrow Fe^{2+} + 2e^- \\ Cr &\rightarrow Cr^{3+} + 3e^- \end{aligned} \qquad (7)$$

Some dissolved metal ions further hydrolyse and the pH value can be reduced due to the following reactions:

$$\begin{aligned} Fe^{2+} + 2H_2O &\rightarrow Fe(OH)_2 + 2H^+ \\ Cr^{3+} + 3H_2O &\rightarrow Cr(OH)_3 + 3H^+ \end{aligned} \qquad (8)$$

The accumulation of more cations further promote the migration of more chloride ions to the corrosion site, resulting in an acid environment and the continuous dissolution of the metals. As a result, the pitting nuclei develop into obvious pitting pits and the surrounding areas are protected. Meanwhile, the observed irregular convex area can be attributed to the diffusion process. Some dissolved metal ions diffuse outwards through the thin water layer and the precipitation reaction occurs at a place with a high enough pH.

3.2. Tribological performance

Fig. 7(a) shows the COF evolution of the DLC coatings during the reciprocating sliding process, and the average COF in the steady state (excluding the sliding process before 250 s) is provided in Fig. 7(b). During the short sliding process, the COF of the sample S1 is higher than that of the sample S0. After a sliding time of 1000 s, the COF of the sample S1 decreases and the average COF in the steady state is slightly lower than that of the sample S0. For the other samples, the COF is always lower than that of the sample S0, and the average COF decreases with the increasing accidental damage on the coating surface caused by the prefabricated scratches. The average COF of all the samples is stable between 0.14 and 0.21. The sample S0 shows the highest average COF of 0.21. Compared with that, the average COF of the samples S1–S6 are 0.2, 0.18, 0.17, 0.17, 0.15 and 0.14, respectively. The COF is the ratio of shear stress to contact stress, and the reduced shear property between the wear pairs is the main reason for improving the antifriction performance of the coating. Compared with the COF of the sample S0, the reduction in COF of the samples S1–S6 could be related with the microstructural evolution due to the GCr15 grinding pair reciprocated sliding across the prefabricated scratches. The wear rate of the DLC coatings after the reciprocating sliding process can also be seen in Fig. 7 (b). The wear rate of the sample S0 is 2.265×10^{-16} $m^3/(N \cdot m)$ and this increases slightly to 2.375×10^{-16} $m^3/(N \cdot m)$ and 2.409×10^{-16} $m^3/(N \cdot m)$ for the samples S1 and S3, respectively. The wear resistance of the samples S4–S6 obviously decreases and the wear rate of the sample S6 increases to 5.301×10^{-16} $m^3/(N \cdot m)$, which is twice as much as that of the sample S0. Meanwhile, the sample S2 shows excellent wear resistance with the lowest wear rate of 1.848×10^{-16} $m^3/(N \cdot m)$, which indicates that the wear resistance of the coating can be improved with an appropriate scratch damage structure acting on the surface.

Raman spectroscopy is an effective method to investigate the structural feature of DLC coatings. Fig. 8 shows the Raman spectra of the wear tracks on the coatings and the corresponding ID/IG ratio. As observed from Fig. 8(a), the Raman peaks of the wear tracks on the samples S0–S6 reveal a similar trend. It can be deconvoluted into the D peak at around 1350 cm^{-1} and the G peak at around 1580 cm^{-1} using Gaussian curve function. As shown in Fig. 8(b), the Gaussian fitting results and the ratio of ID/IG illustrate the changes of C–C sp^2 bond and C–C sp^3 bond contents in the DLC coatings [26]. In the curve, the final ID/IG ratio of each sample was determined by averaging values at four different points on the wear track, and the error bar indicates the deviation error from the average value of four tests. The ID/IG ratio of the sample S0 is 0.894 ± 0.023, which increases from 1.011 ± 0.013 to 1.177 ± 0.038 for the samples S1, S3–S6. Compared with the sample S0, the higher ID/IG ratios of the S1, S3–S6 samples indicate a better lubrication effect with a higher content of C–C sp^2 bonds. During the sliding process, the transformation of coating structure towards graphitization, in turn, reduces the shear stress and COF. Meanwhile, the lowest ID/IG ratio of the sample S2 indicates that the special scratch damage structure of the coating surface is not conducive to graphitization, which may accelerate the reduction of the ID/IG ratio.

Fig. 9. shows the surface morphologies and wear tracks section (non-scratching region on wear tracks) of the coatings after the reciprocating sliding process. It can be seen that the bulges on both sides of the scratches were removed for all the samples. Compared with the sample S0, the minimum wear section area of 20.21 um2 can be observed for the sample S2. Comparatively, the poor wear resistance with increased wear section area appears on the other samples.

Remarkably, the wear rate trends of the samples S1, and S3–S6 are contrary to the COF results. After the sliding process, the graphitization transformation of the coating structure reduces the shear stress and COF. Meanwhile, as a result of graphitization, the coating surface softens, resulting in the poor wear resistance and higher wear rate [15]. It has been proven that the mechanical properties of the wear track have a great influence on the wear performance. For the sample S2, the special scratch damage structure may contribute to the excellent tribological performance, which will be further discussed in the following section. The SEM microscopic morphologies of the wear tracks on the DLC coatings are also shown in Fig. 9. It is worth noting that obvious wear debris particles are detected on the wear scar surfaces of the samples S0–S1 and S3–S6. During the friction process, the high contact pressure generated by wear debris can cause graphitization transformation and the wear debris particles can also scratch the coating surface, thus, the related abrasive wear mechanism causes the higher wear rate and wear volume. Comparably, most wear debris particles cannot be detected on the wear scar surface of the sample S2. The phenomenon illustrates that the surface structure of the sample S2 can act as a debris collector [27,28]. Almost invisible debris occupy the main role of making a smoother surface, avoiding serious abrasive wear and graphitization due to the low contact stress, thus improving the tribological performance with lower COF and wear rate [29].

To investigate the mechanical properties of the wear tracks on the coatings, the nanoindentation tests are used to acquire the information of hardness (H), the ratios of H/E and H3/E [2], which are shown in Fig. 10. From Fig. 10(a), it is obvious that the sample S0 shows the H value of 15.35 ± 0.51 GPa. Compared with that, the reduced hardness H_{ri} can be express as:

$$H_{ri} = Hi/H - 1 \quad (9)$$

where H is the nano-hardness value of the sample S0.

The sample S2 exhibits excellent mechanical properties with the maximum H of 18.68 ± 1.28 GPa and a positive reduced hardness of 0.22. With the exception of the sample S2, the H values of the other samples are all lower than that of the sample S0, resulting in the negative reduced hardness. It has been reported that the ratios of H/E and H3/E2 can well represent the durability and plastic deformation resistance of the coating [30]. From Fig. 10(b), the H/E and H3/E2 values gradually decrease for the samples S1, S3–S6 and these are all lower than those of the sample S0. The variation of these values can be elucidated by the evolution of the microstructure during the whole sliding process. Meanwhile, the outstanding durability and plastic deformation resistance with the highest H/E and H3/E2 values can be observed in the wear tracks on the sample S2, resulting in a better wear resistance.

The schematic illustration of the tribological mechanism is shown in Fig. 11. As shown in Fig. 11(a), for the sample S0, the wear debris particles produced during the sliding process exist on the surface of wear tracks, leading to a certain degree of abrasive wear. For the samples with scratch damages, the wear debris particles are consist of two major sources: natural generation during the sliding process and the bulges on both sides of the scratch. To maintain the appropriate scratch width or the ratio of the scratch width to the contact width is important to the tribology performance of the coatings. According to Hertz contact theory, the contact width is about 0.357 mm. The ratios of the scratch width to the contact width for samples S1–S6 are 0.033, 0.241, 0.317, 0.412, 0.462 and 0.515, respectively. If the scratch width is smaller or the

ratio of the scratch width to the contact width is lesser as the sample S1 (scratch width of 0.012 mm and the ratio is 0.033), most of the wear debris particles can cross the scratch area and exist on the surface of the wear tracks, resulting in an unobvious function acting as reservoirs. Meanwhile, if the scratch width is larger or the ratio of the scratch width to the contact width is greater as the sample S6 (scratch width of 0.184 mm and the ratio is 0.515), the decreased actual contact surface and the increased average contact pressure at the sliding interface can lead to severe wear and more wear debris. The more wear debris exceed the storage capacity of the scratches and as a function of abrasive wear, resulting in the significant reduction in tribology performance. To maintain the ratio of the scratch width to the contact width at approximately 0.24 as the sample S2 is more effective for entrapping the most wear debris and obtaining the excellent tribology performance.

4. Conclusions The aim of this paper is focused on the influence of different types of surface damage on the anticorrosion and tribological performances of the DLC coating. After the corrosion and tribological tests, the main conclusions are summarized as follows:

(1) On the basis of improving the total Pol R of the stainless steel substrate, cracking or spalling of the coating caused by accidental damage promotes the corrosion failure of the coating system and the pitting corrosion of the stainless steel substrate. As a result, the I_{corr} of 2.880×10^{-8} (A/cm^2) as the sample S6 is one order of magnitude higher than the continuous and complete state as the sample S0 (1.181×10^{-9} (A/cm^2)).

(2) Compare with the sample S0, the other samples with scratch damages present different tribological performances. Except for the sample S2, the gradually reduced COF and weakened wear resistance can be observed for the samples S1, S3–S6. (3) With the special scratch width (0.012 mm) and the ratio of the scratch width to the contact width (0.033), the sample S2 shows the lowest ID/IG (0.846), highest H/E (0.109) and H3/E2 (0.221) values, which effectively avoid the softening of coating surface caused by graphitization and improve the durability and plastic deformation resistance. Meanwhile, the effective collection of wear debris particles makes an excellent tribological performance with the lowest wear rate of 1.848×10^{-16} m3/(N ·m).

CRediT authorship contribution statement

Yefei Zhou: Conceptualization, Methodology, Writing-original draft. **Lulu Li:** Data curation, Analysis, Investigation. **Zhihao Chen:** Data curation, Validation. **Lixiang Rao:** Methodology. **Xuejun Ren:** Validation. **Xiaolei Xing:** Supervision, Project administration, Funding acquisition. **Qingxiang Yang:** Writing-review & editing.

Declaration of competing interest

The work described has not been submitted elsewhere for publication, in whole or in part, and all the authors listed have approved that the manuscript is enclosed. The authors would like to express their gratitude for projects supported by the National Natural Science Foundation of China (Grant Nos. 51705447 and 51905466), P. R. China, Youth Top Talent Project of Hebei Province Higher Education (Grant No. BJ2019058) and Natural Science Foundation of Hebei Province China (E2020203184).

Acknowledgements This work was supported by the National Natural Science Foundations (Grant Nos. 51705447 and 51905466), P. R. China, Youth Top Talent Project of Hebei Province Higher Education (Grant No. BJ2019058) and Natural Science Foundation of Hebei Province China (E2020203184).

Table 1
Deposition process parameters of the DLC coating.

Deposition process	Ion beam voltage (V)	Bias voltages (V)	The gas flow of Ar (sccm)	The gas flow of C_2H_2 (sccm)	Cr target current (A)	C target current (A)	Deposition time (min)	Thickness (μm)
Cr	1300	600	30		2		60	
CrC	1300	600	30		2	2	60	2.4
DLC	1300	600	30	60		3	180	

Table 2
Polarization parameters of DLC coatings and stainless steel substrate.

Samples	E_{corr} (V)	I_{corr} (A/cm^2)	Pol R (Ω)
S0	−0.190	1.181×10^{-9}	2.897×10^{7}
S1	−0.261	1.796×10^{-9}	2.202×10^{7}
S2	−0.205	2.347×10^{-9}	1.486×10^{7}
S3	−0.202	5.029×10^{-9}	6.354×10^{6}
S4	−0.200	5.129×10^{-9}	6.313×10^{6}
S5	−0.219	1.958×10^{-8}	1.703×10^{6}
S6	−0.242	2.880×10^{-8}	1.627×10^{6}
Stainless steel substrate	−0.346	2.901×10^{-8}	1.199×10^{6}

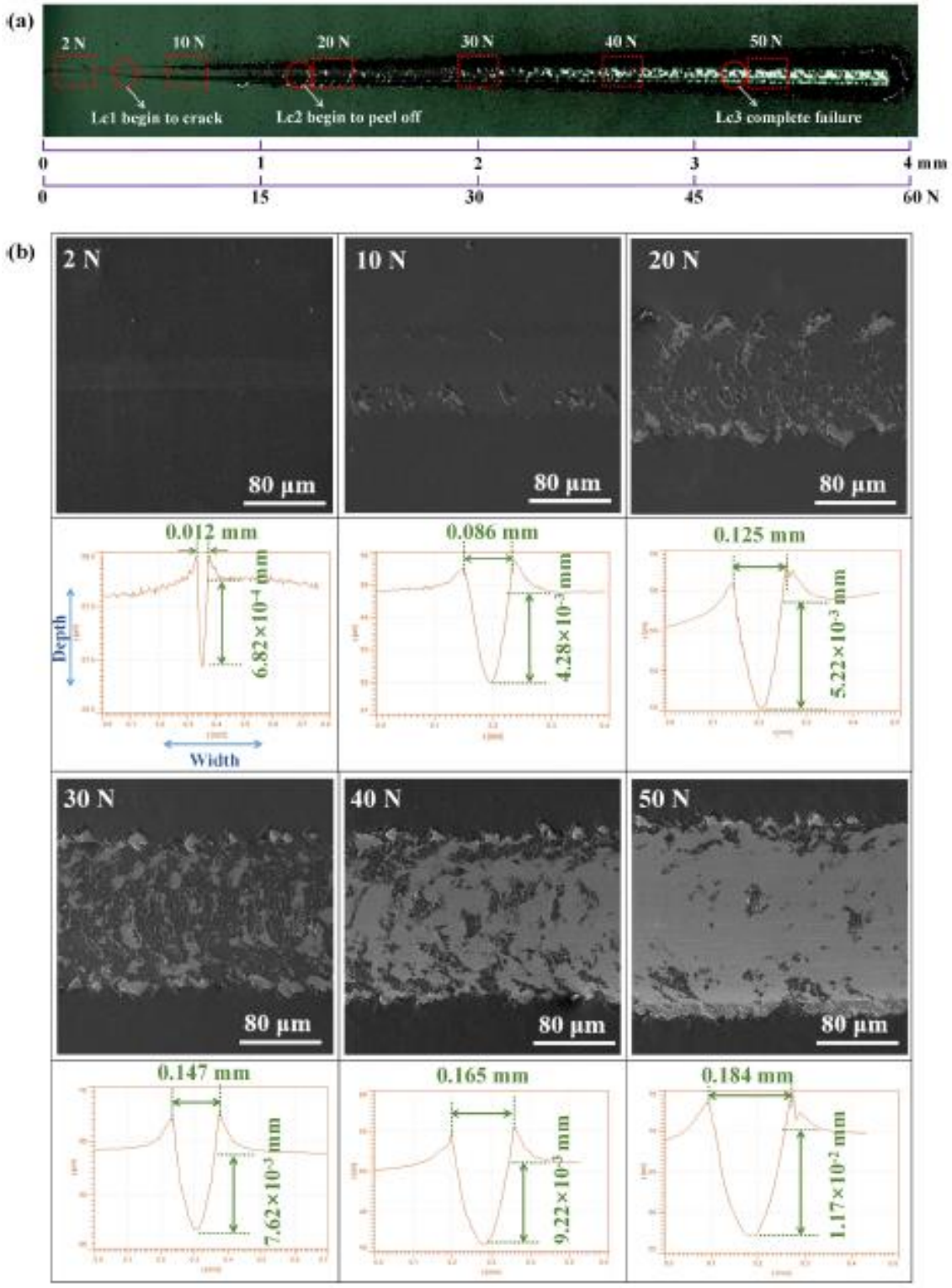

Fig. 1. Scratch tracks of the DLC coating: (a) Adhesion behavior result; (b) SEM morphologies and section parameters of the coatings with different scratch loads.

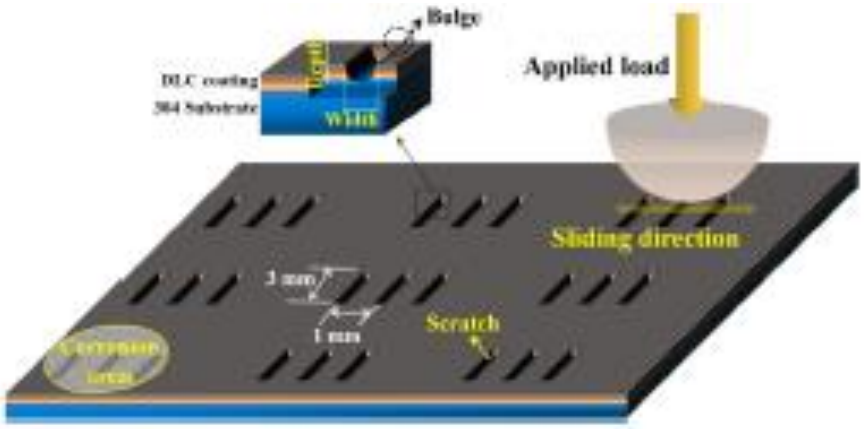

Fig. 2. Schematic illustration of the scratches on the DLC coating surface and the processes of corrosion and tribological tests.

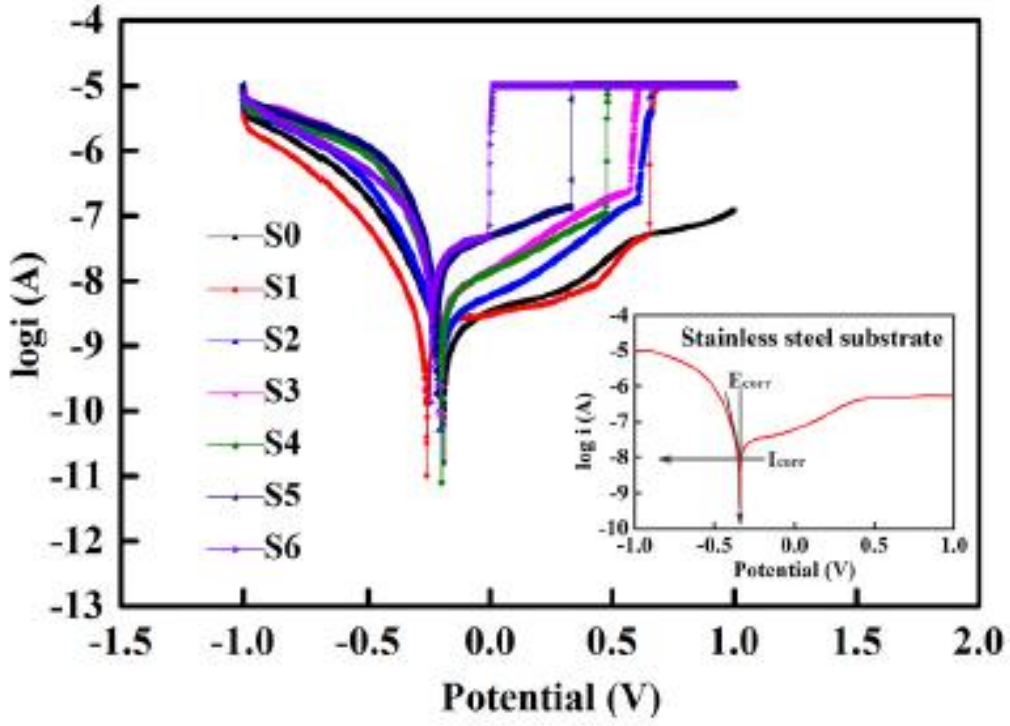

Fig. 3. Potentiodynamic polarization curves of the DLC coatings.

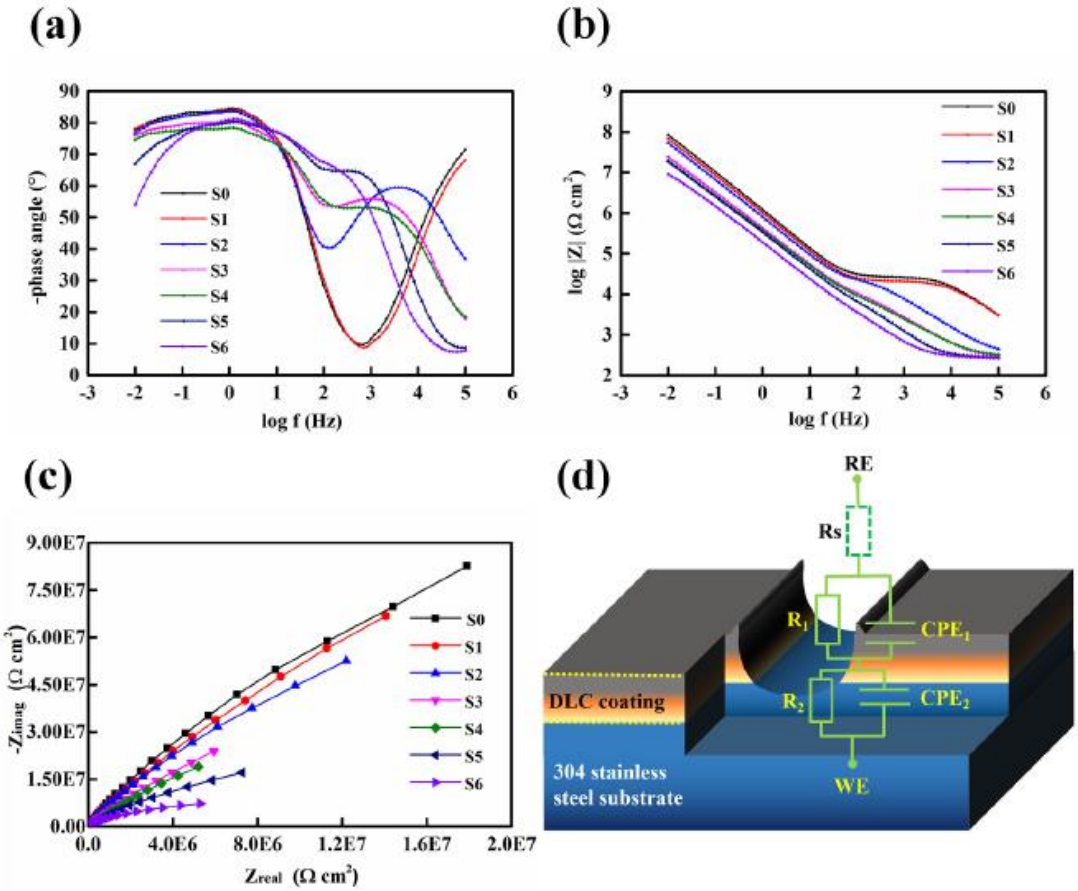

Fig. 4. EIS results of the DLC coatings: (a) Bode-phase; (b) Bode-impedance; (c) Nyquist; (d) Equivalent circuit model.

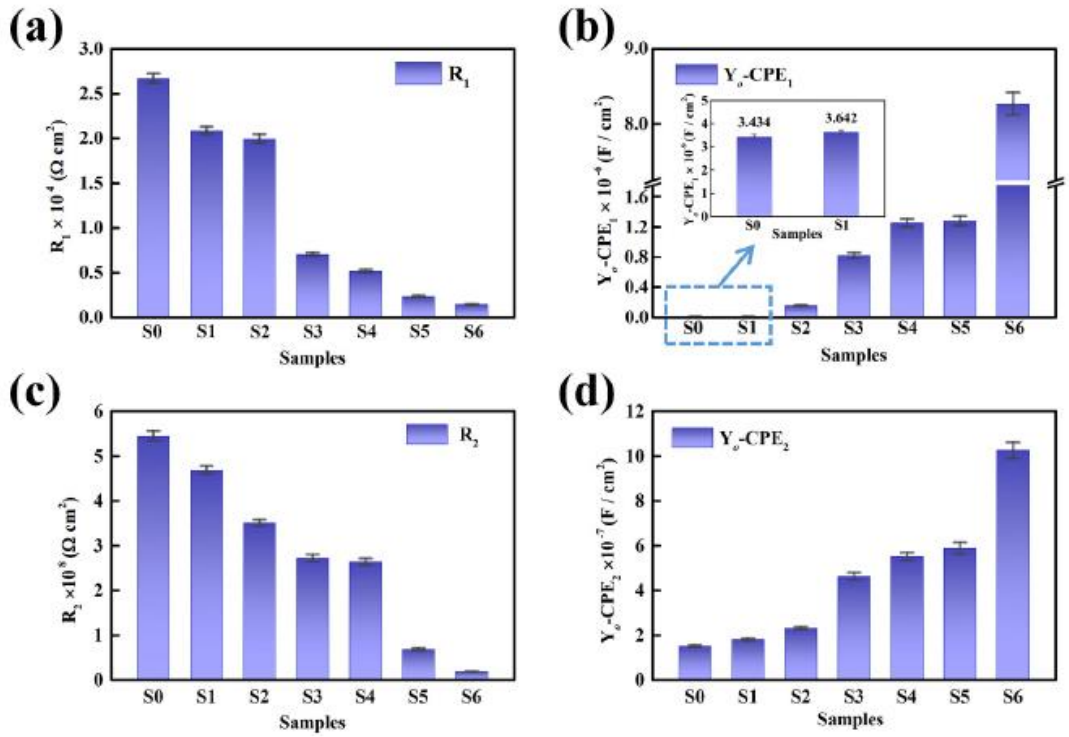

Fig. 5. Specific electrochemical parameters obtained from the equivalent circuits: (a) R1; (b) CPE1; (c) R2; (d) CPE2.

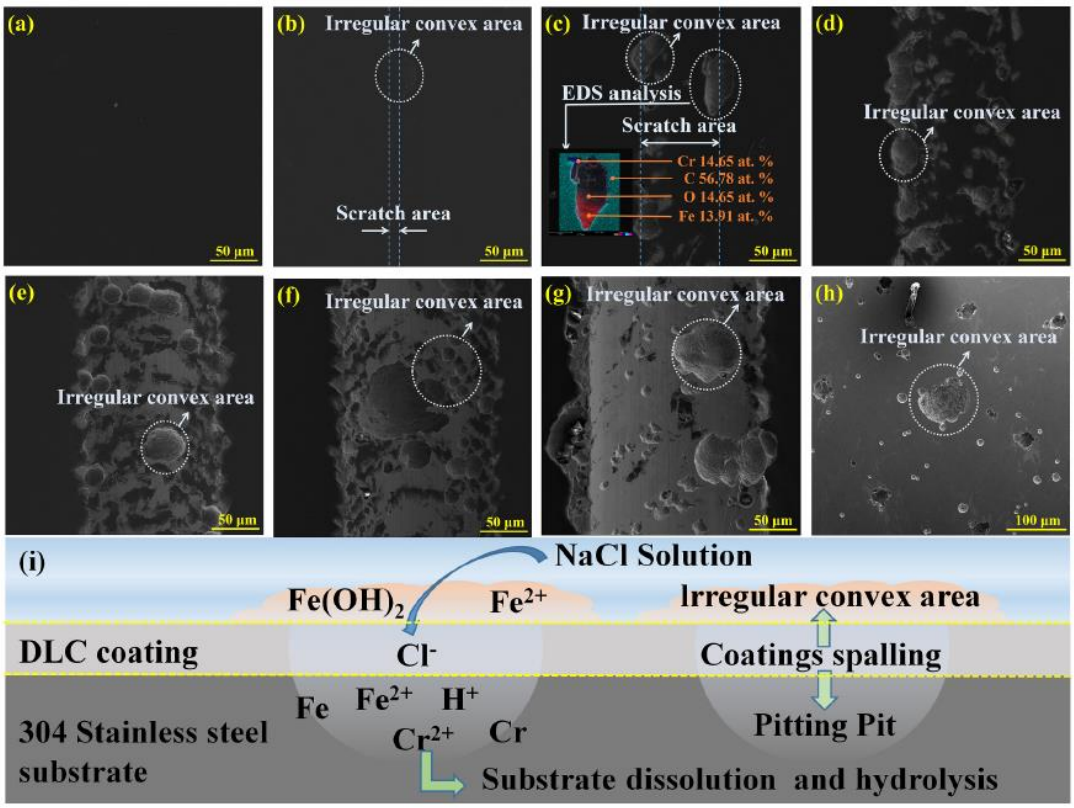

Fig. 6. SEM morphologies of the DLC coatings after potentiodynamic polarization tests and pitting corrosion mechanism on the stainless steel substrate: (a) S0; (b) S1; (c) S2; (d) S3; (e) S4; (f) S5; (g) S6; (h) Stainless steel substrate; (i) corrosion mechanism.

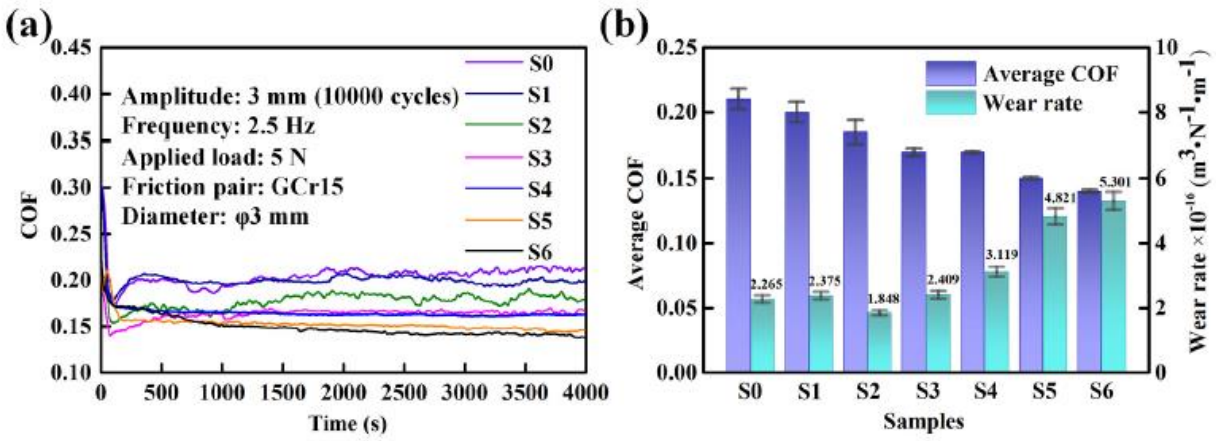

Fig. 7. Friction coefficients and wear rate results of the DLC coatings.

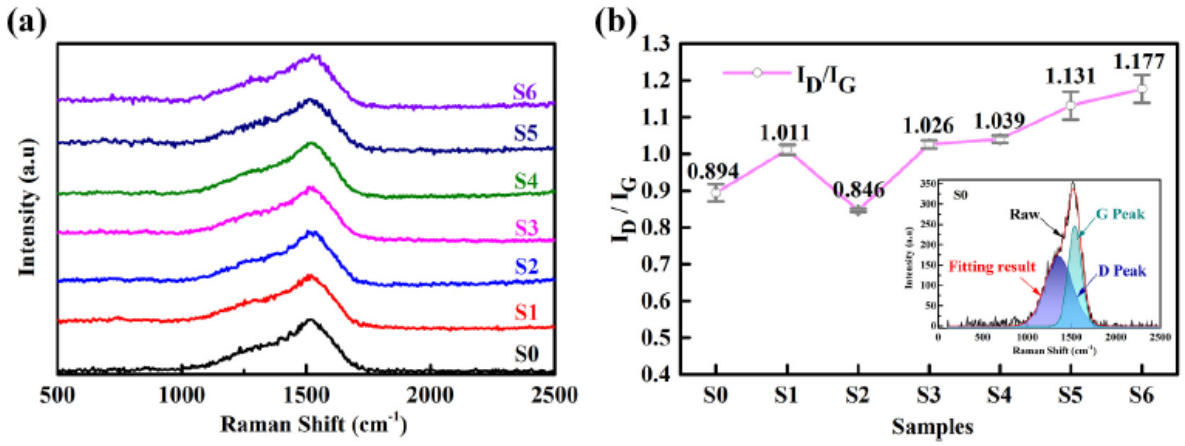

Fig. 8. Raman results of the wear tracks on the DLC coatings: (a) Raman spectra; (b) ID/IG ratio.

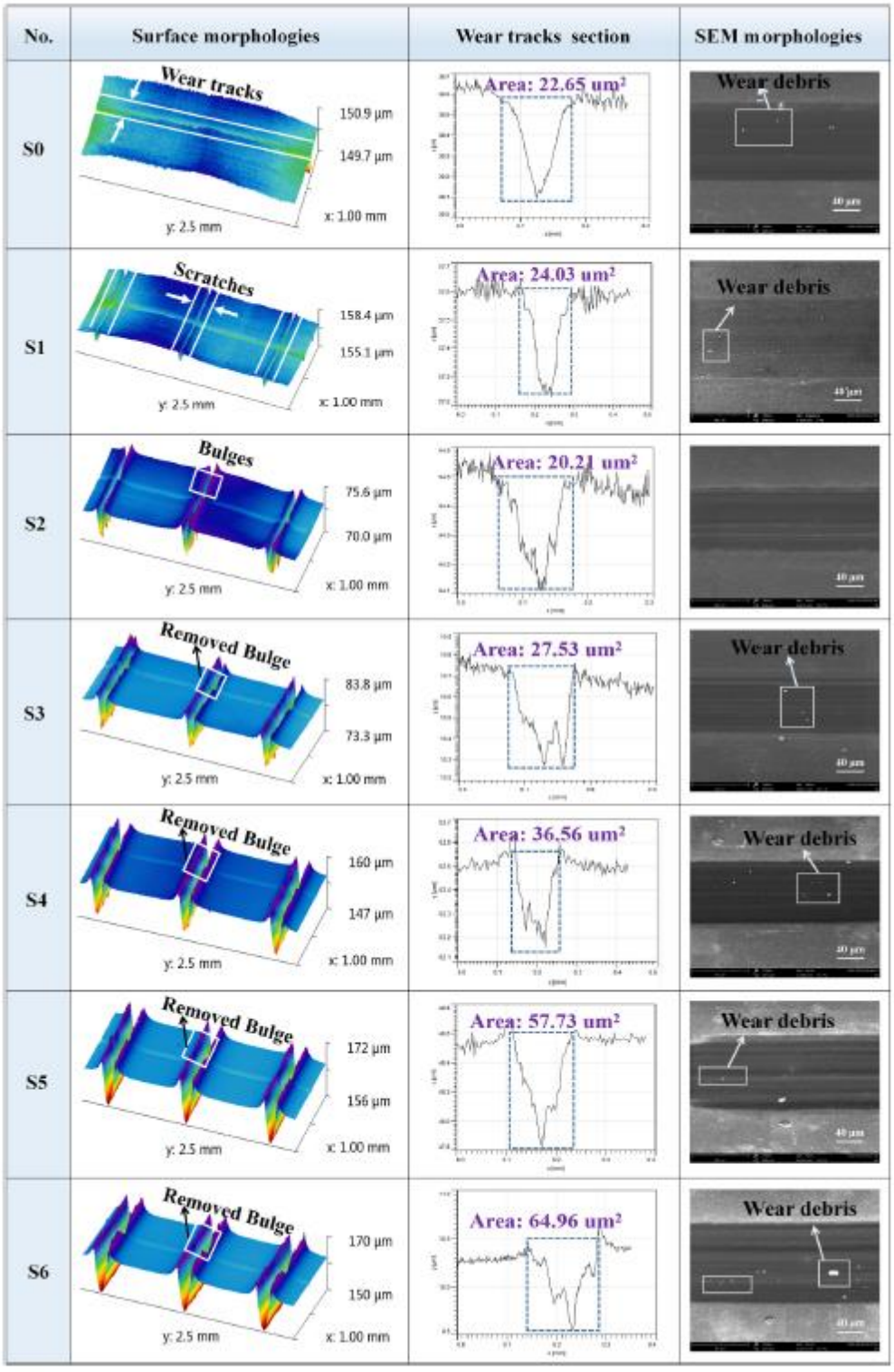

Fig. 9. Surface morphologies, SEM and section images of wear tracks on the DLC coatings after the reciprocating sliding process.

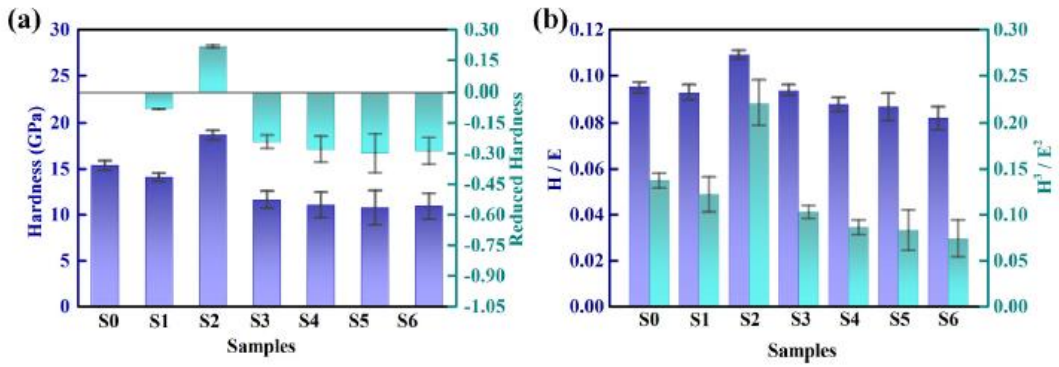

Fig. 10. Mechanical properties of the wear tracks on the DLC coatings: (a) H and *Hri*; (b) H/E and H3/E2 ratios.

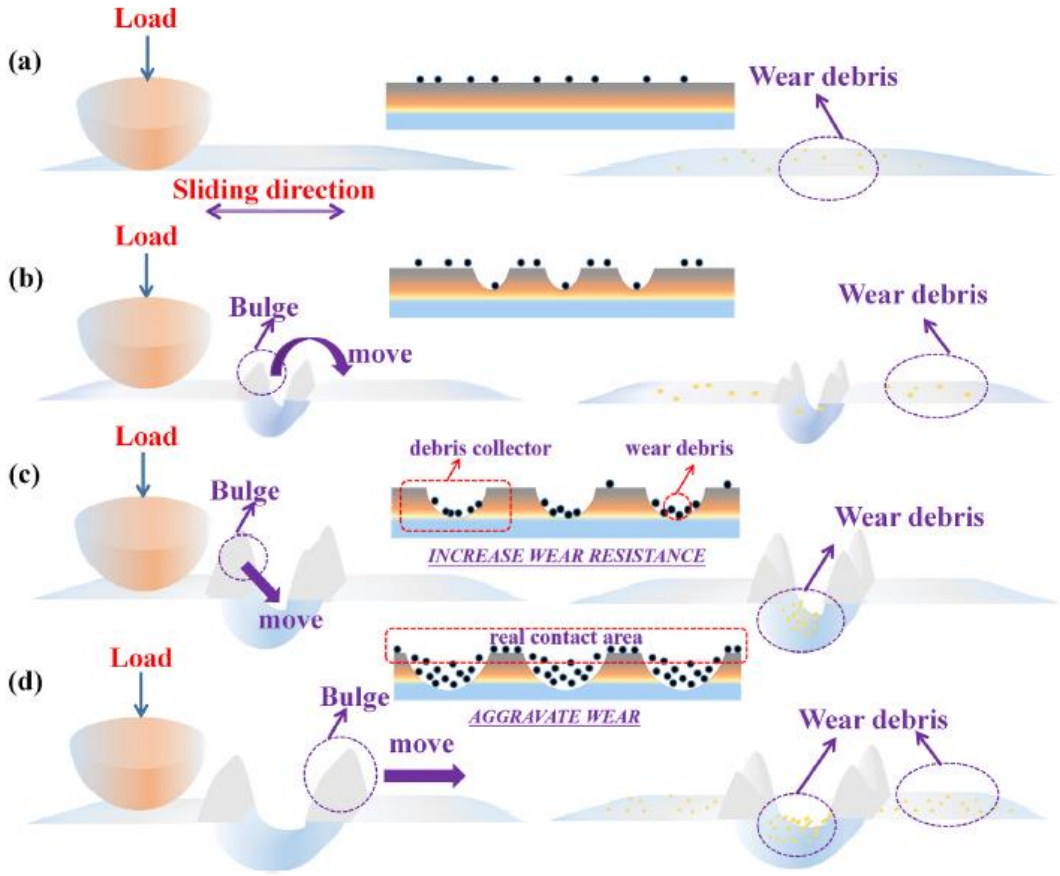

Fig. 11. Schematic illustration of tribological mechanism: (a) S0; (b) S1; (c) S2; (d) S6.